

Supplementary Information for:

**Controlling the Roll-to-Helix Transformation in  
Electron-Beam-Patterned Gel-Based Micro-Ribbons**

Xinpei Wu,<sup>1</sup> Teng Zhang,<sup>2</sup> and Matthew Libera<sup>1</sup>

<sup>1</sup> Department of Chemical Engineering and Materials Science  
Stevens Institute of Technology  
Hoboken, NJ USA 07030

<sup>2</sup> Dept. of Mechanical and Aerospace Engineering  
Syracuse University  
Syracuse, NY USA 13244

## 1. Materials and Methods

**Materials:** Poly(acrylic acid) [PAA; average  $M_w = 450,000$  Da; Sigma Aldrich], Phosphate Buffered Saline [PBS; Sigma Aldrich], Hydrochloric acid [ACS reagent,  $\geq 37.0\%$ ; HCl; Sigma Aldrich], Sodium chloride [ACS reagent,  $\geq 99.0\%$ ; NaCl; Sigma Aldrich], 3-(Trihydroxysilyl)-1-propanesulfonic acid (30-35% in water; Sulfonic acid-silane; Gelest), 1-ethyl-3-(3-dimethylaminopropyl)carbodiimide hydrochloride [EDC; Thermo Scientific], N-hydroxysulfosuccinimide [Sulfo-NHS; Thermo Scientific], 5-Aminofluorescein [Amine-FITC; Sigma Aldrich] and Cyanine3 amine [Amine-Cy3; Lumiprobe] were used as received. Type I deionized (DI) water was provided by a Millipore Direct Q system. Phosphate buffer with pH = 7.4 was prepared by diluting PBS 10 times (0.1X PBS), and phosphate buffer at pH 3.0 was prepared by adding hydrochloric acid to 0.1X PBS to adjust pH to 3.0. In both cases, the ionic strength was  $[Na^+] = 0.0148$  M.

**Silane surface treatment:** Silicon wafers (5 mm  $\times$  5 mm, Ted Pella) were immersed in piranha solution (3:1 H<sub>2</sub>SO<sub>4</sub>/H<sub>2</sub>O<sub>2</sub>, use with caution) overnight, then rinsed multiple times with DI water and dried with gently flowing nitrogen gas. These wafers were then immediately exposed to oxygen plasma for 10 min. The wafers were immersed in 2 % (v/v) sulfonic acid-silane in ethanol for 10 min. After rinsing twice in ethanol, the silane-treated wafers were baked in air for 2 hr at 120 °C.

**Fabrication of fluorescently labelled PAA films:** Carbodiimide chemistry was used to prepare fluorescently labelled PAA. Following the manufacturer's protocol, 1 mg EDC and 1.7 mg Sulfo-NHS were added to 2 ml of PAA solution (4 wt % in methanol) to activate the carboxylic acids. The mixture was sonicated for 15 min at room temperature. Then, 50  $\mu$ l of amine-Cy3 solution (1 mg/ml in MES buffer) was vortexed with 2 mL of activated PAA solution. The ratio of amine-Cy3 to PAA targeted the labelling of 0.005% of the PAA carboxyl groups. After 1 hr of reaction, polymer films were prepared by dropping 50  $\mu$ l of labelled PAA solution onto silane-treated Si substrates spinning at 5000 rpm for 20 sec.

**E-beam patterning ribbons:** E-beam lithography was carried out using a Thermo Fisher Scientific Apreo 2S field-emission gun scanning electron microscope (FE-SEM). This FE-SEM was equipped with a high-speed electron beam-blanking system and a Nanometer Pattern Generation System (NPGS, JC Naby Lithography Systems). Shape-shifting patterns were created using focused electron beams with  $E_0 = 2$  keV and a beam current of  $\sim 400$  pA. The interpixel spacing along the  $\hat{x}$  and  $\hat{y}$  directions was held constant at 4.84 nm. Rectangular tethering pads (20  $\mu$ m  $\times$  1  $\mu$ m) were then patterned using 10 keV electrons with a beam current of  $\sim 400$  pA. The tethering pads were patterned using an interpixel spacing in the  $\hat{x}$  and  $\hat{y}$  directions of 200 nm. The tethering neck was fabricated using 2 kV electrons to pattern a 8  $\mu$ m line with point dose of 100 fC connected to the tethering pad and a 2  $\mu$ m line with point dose of 4 fC connected to the ribbon. These two lines were also connected to each other. Point doses,  $D_p$ , (the total number of electrons per pixel), for patterning the shape-shifting ribbons ranged from 0.5-3 fC. Patterning a 2  $\mu$ m  $\times$  40  $\mu$ m rectangle required a total exposure time on the order of 8 sec, depending on the point dose. The slowest step in the processing corresponded to the electron microscope realignment required when

changing the accelerating voltage from 2 keV to 10 keV. After exposure, insufficiently cross-linked polymer was removed by immersing the substrates in 2–3 mL of phosphate buffer (pH = 3;  $[\text{Na}^+] = 0.0148 \text{ M}$ ) for 10 min with gentle rotary shaking (30 rpm). After rinsing twice, the patterned wafers were immersed in low-ionic-strength ( $[\text{Na}^+] = 0.0148 \text{ M}$ ) pH 3 or pH 7.4 phosphate buffer for the subsequent imaging. The specimens were not allowed to dry.

**Post-labelling experiments:** Carbodiimide chemistry was used again to post-label the carboxyl groups in the developed ribbons. 1 mg EDC and 1.7 mg Sulfo-NHS were added to 2 ml pH 3 buffer and vortexed for 1 min. 30 ml of the mixed solution was dropped onto the hydrated ribbons tethered to a silicon wafer and kept for 15 min at room temperature. After the activation of the carboxyl groups, the wafer was rinsed twice using pH 3 buffer. Then, 30  $\mu\text{l}$  of Amino-FITC solution (1 mg/ml in pH 3 buffer) was dropped onto the rinsed sample. After 1 hr of reaction, the sample was rinsed 3 times for 10 min with gentle rotary shaking (30 rpm).

**Characterization:** Confocal images were collected using a Nikon Ni-E upright microscope equipped with an AxR confocal system with a Nikon Water Dipping 60X objective lens (CFI Fluor 60X W, NA 1.0 and W.D. 2.0 mm). 3D-stacked images were collected with a typical z-step of 0.3  $\mu\text{m}$ . Confocal images were extracted using the Fiji image-processing software. 3D visualization and image quantification were implemented using the 3D Viewer plugin for Fiji and NIS-Elements C software. Images were collected in phosphate buffer with pH values of either 3.0 or 7.4 at a fixed ionic strength ( $[\text{Na}^+] = 0.0148 \text{ M}$ ).

**Modelling:** We performed all simulations with the ABAQUS/implicit solver. The region 1 and 2 (hard) material and the region 3 (soft) material were modelled using the isotropic elastic material model in ABAQUS under geometric nonlinear deformation. We assumed that the Young's moduli of the hard and soft regions were 100 MPa and 1 MPa, respectively, and their Poisson ratios were 0.3 and 0.4, respectively. We assumed a total ribbon thickness of 500 nm. The thickness of the hard material was used as a tuning parameter to match the experimentally measured bending radius of a ribbon with a length less than 20  $\mu\text{m}$ . The swelling behavior was modelled as a volumetric expansion and implemented through the thermal expansion function in ABAQUS. Based on prior experimental measurements,<sup>21</sup> we used a linear swell ratio of 1.2 (20% swelling at pH 3).

We modelled tiled ribbons using two different assumptions. One assumed a homogeneous material in the gaps between tiles with a gap thickness of 200 nm. This material was assumed to swell uniformly (20% linear expansion). To reduce computational cost, we assumed a gap thickness of 200 nm with a modulus of 0.1 MPa rather than the thickness measured experimentally ( $\sim 20 \text{ nm}$ ) with a modulus of 1 MPa as assumed above for our model of the region 3 material. This configuration corresponded to a structure with in-plane mechanical anisotropy. The other assumed that the gap material was a bilayer with a non-swelling top layer (100 nm thick) with a modulus of 0.1 MPa. The bottom layer (100 nm thick) was assumed to be identical except that was allowed to swell and the extent of swelling (25%) was established by fitting experimental data. This bilayer structure generated a tiled ribbon with asymmetric through-thickness swelling.

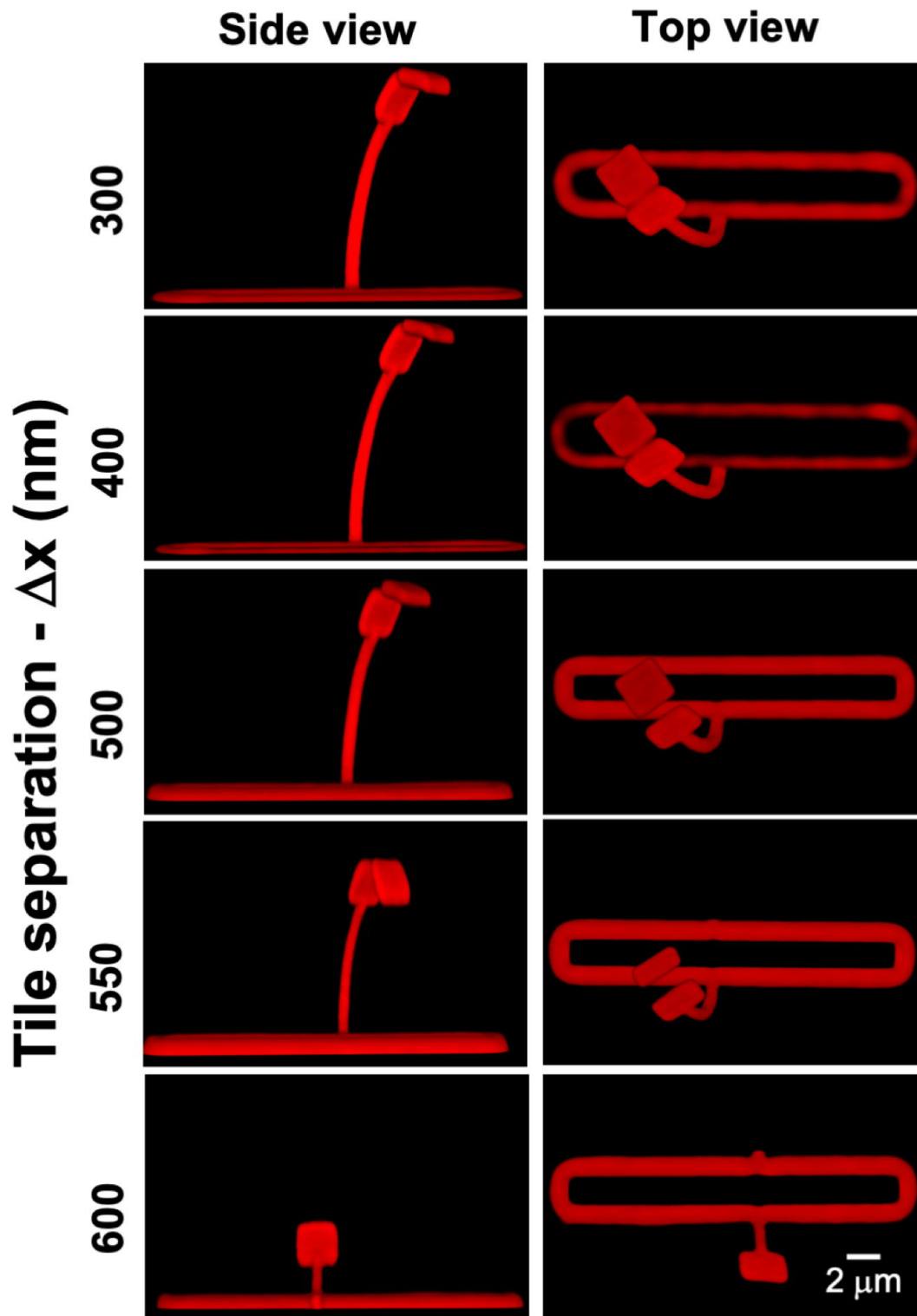


Fig. S1: A tile-separation experiment for  $D_p = 0.5$  fC. Between  $\Delta x = 550$  nm and 600 nm the two tiles become disconnected indicating the lateral extent of proximity effects at this point dose. The samples were each developed and imaged in low-ionic strength ( $[\text{Na}^+] = 0.01$  M) pH 3.0 phosphate buffer.

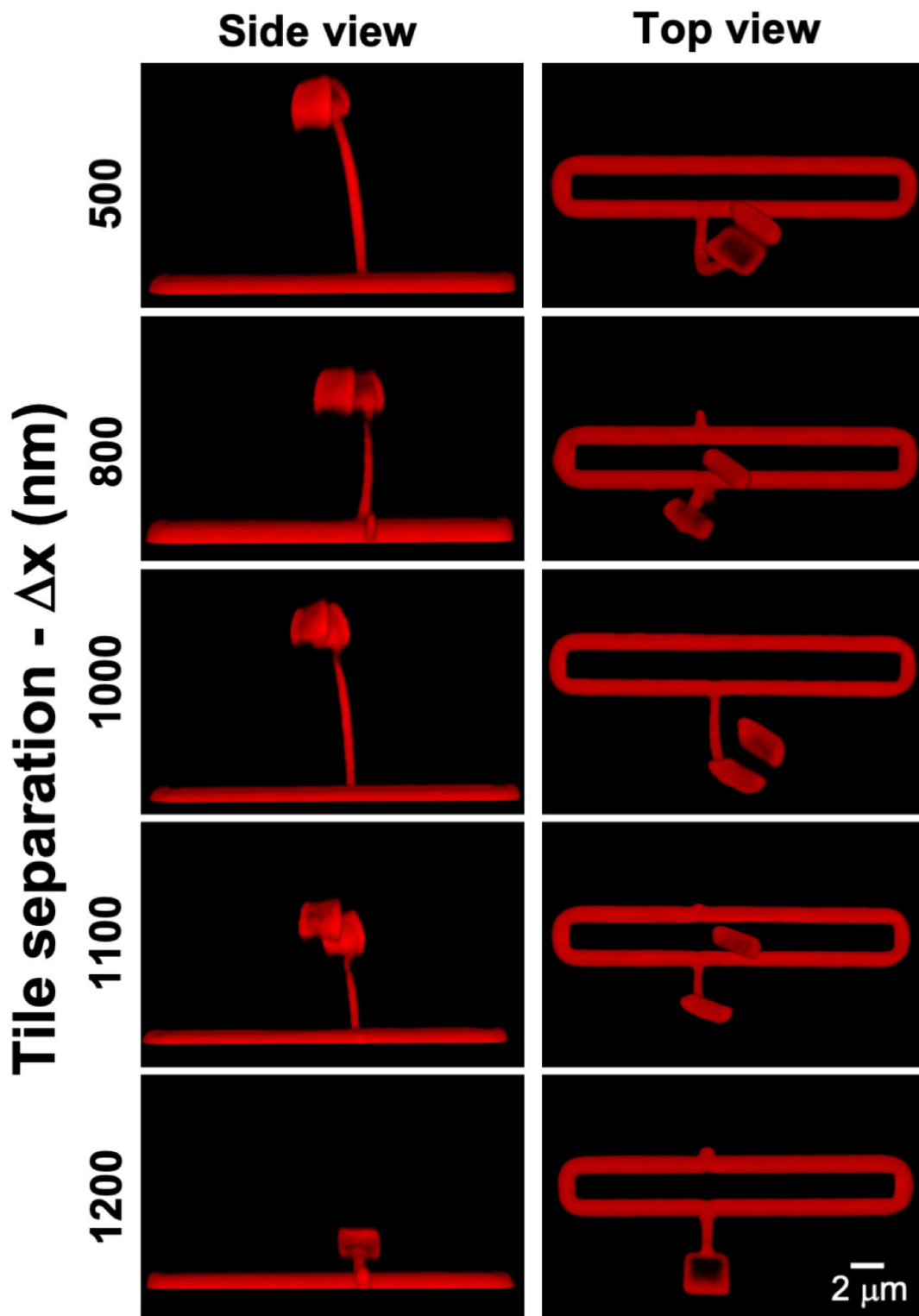


Fig. S2: A tile-separation experiment for  $D_p = 3.0$  fC. Between  $\Delta x = 1100$  nm and 1200 nm the two tiles become disconnected indicating the lateral extent of proximity effects at this point dose. The samples were each developed and imaged in low-ionic strength ( $[\text{Na}^+] = 0.01$  M) pH 3.0 phosphate buffer.

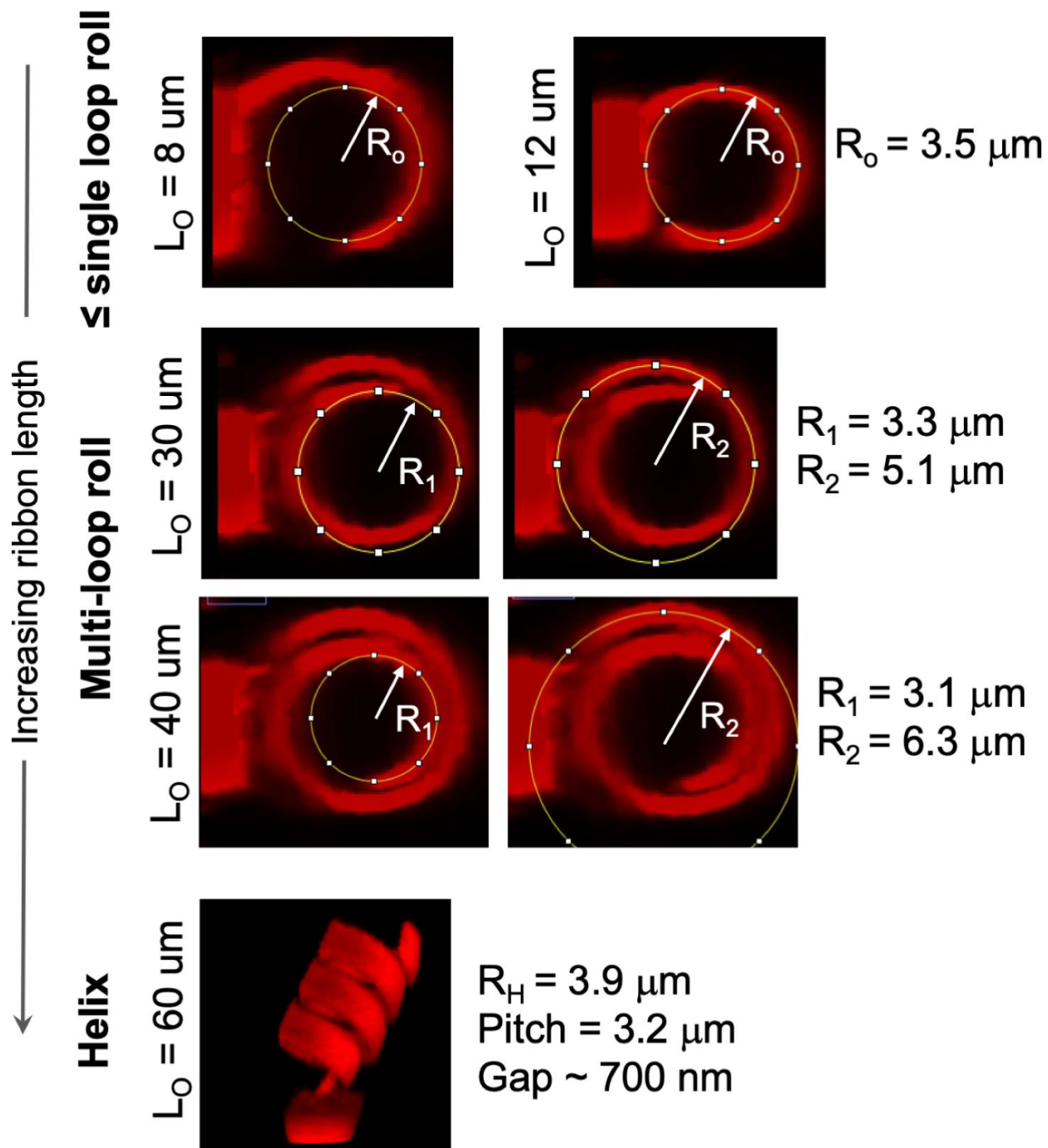


Fig. S3: The various radii associated with: (top) rolls having less than one full loop; (middle) multi-loop rolls; and (bottom) a helical morphology. The ribbons were patterned using a  $D_p$  of 0.5 fC and then developed and imaged in low-ionic-strength ( $[\text{Na}^+] = 0.01 \text{ M}$ ) pH 3.0 phosphate buffer.

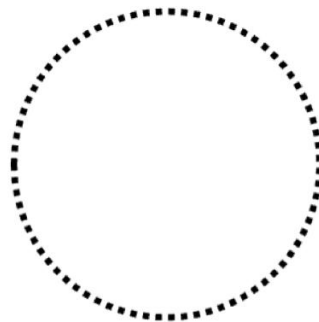
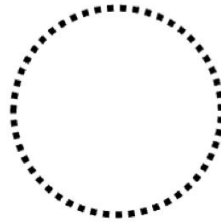
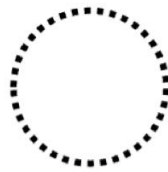
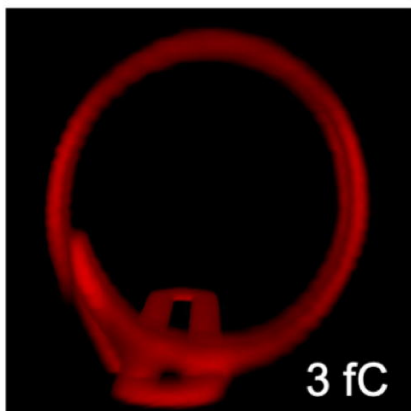
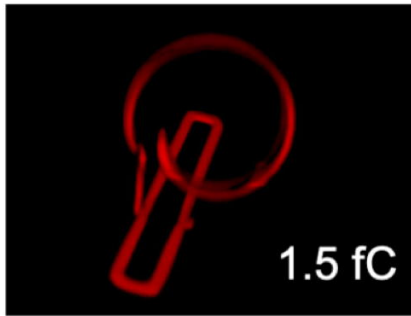
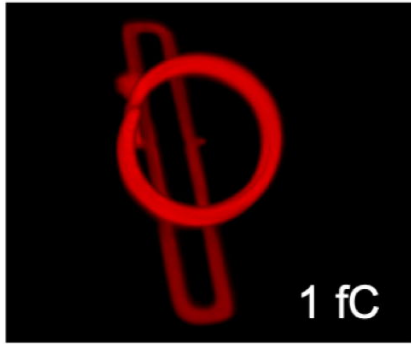
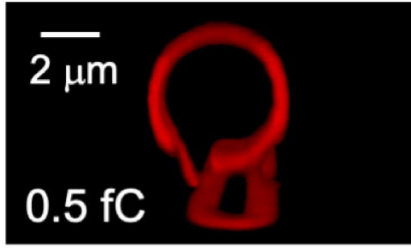


Fig. S4: Increasing the point dose increases the radius of a single-loop roll (developed and imaged in low-ionic-strength ( $[\text{Na}^+] = 0.01 \text{ M}$ ) pH 3.0 phosphate buffer).

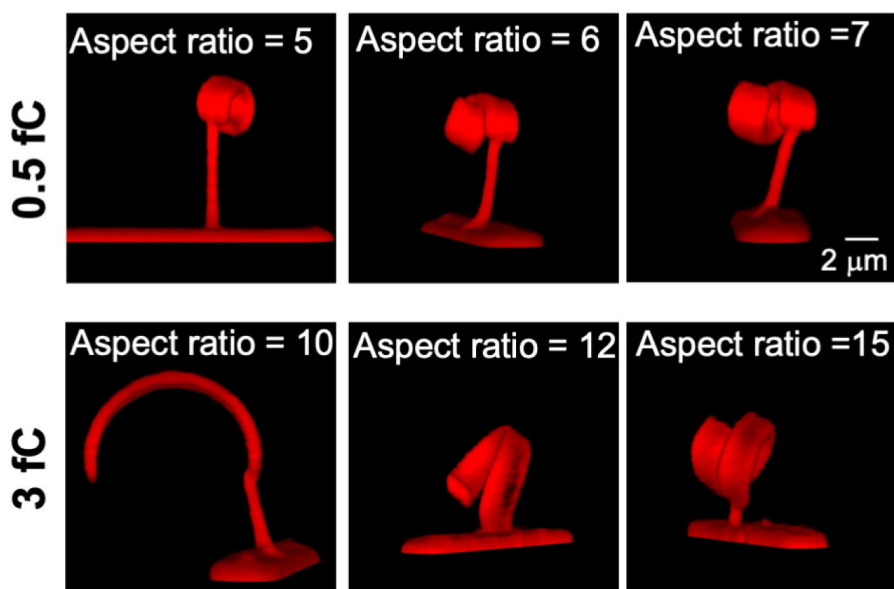
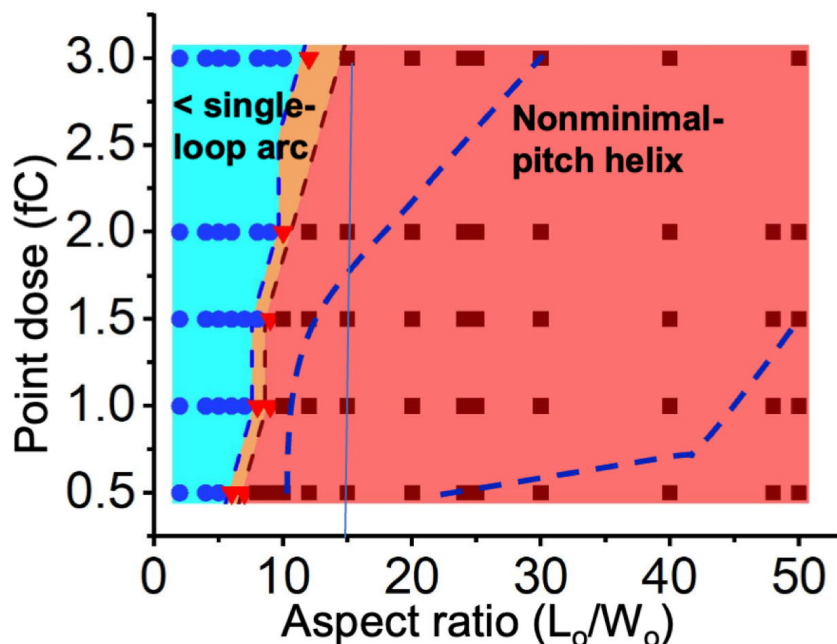
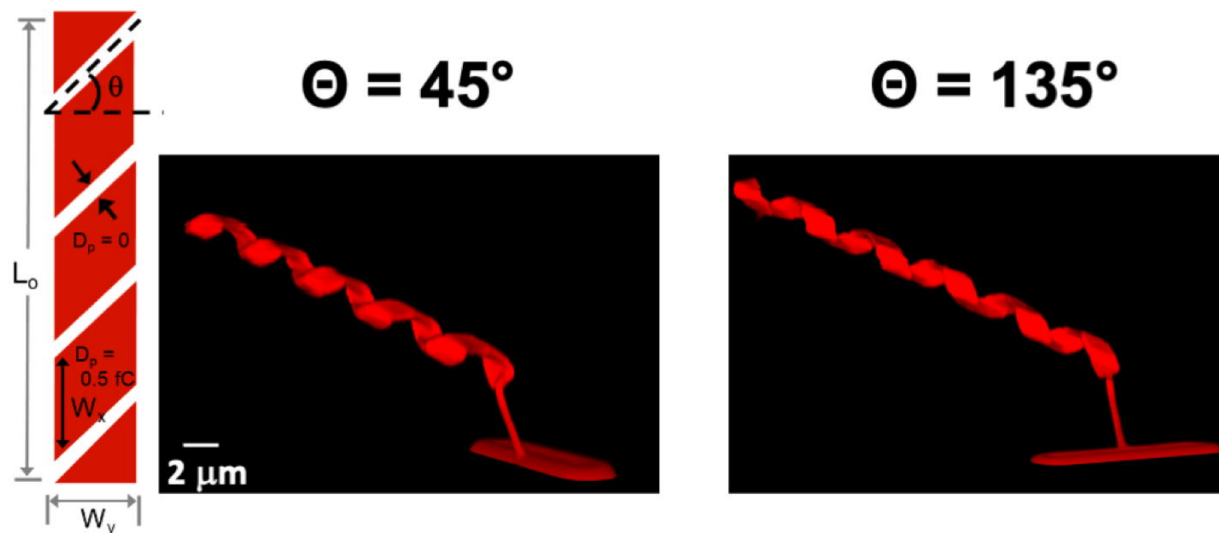


Fig. S5: A morphology map for ribbons patterned using various incident electron doses to create a range of aspect ratios. The ribbons were first developed and imaged at pH 3.0 (see fig. 5 in main manuscript) and then exposed to and imaged in pH 7.4 low-ionic strength ( $[Na^+] = 0.01$ ) phosphate buffer. The two dashed blue lines indicate the left and right sides of the field where the ribbons formed multi-loop rolls at pH 3.0 and then transformed into non-minimal-pitch helices at pH 7.4.

The lower images illustrate, for two different doses, the evolution of morphology across the transition from an arc to a nonminimal pitch helix with increasing ribbon aspect ratio.



**N = 6**

Angle( $^\circ$ )	0	10	30	45	60	90
Chirality	Roll	Left	Left	Left	Left	Roll

**N = 6**

Angle( $^\circ$ )	100	120	135	150	170
Chirality	Right	Right	Right	Right	Right

Fig. S6: Representative images (top) of tiled ribbons with their gap orientations mirrored. The chirality is left-handed for  $\theta = 45^\circ$  and right-handed for  $\theta = 135^\circ$ . The tables (below) indicate, for 6 ribbons at each gap orientation, the chirality is always left-handed for  $10^\circ \leq \theta \leq 80^\circ$  and is always right-handed for  $100^\circ \leq \theta \leq 170^\circ$ .